5th International Conference on Experimental Fluid Mechanics ICEFM 2018 Munich
Munich, Germany, July 2-4, 2018

Estimation of Turbulence Dissipation Rate and Other Statistics from Ensemble PTV Data

Liuyang Ding[*†], **Ronald J. Adrian**

Arizona State University, School of Engineering for Matter, Transport and Energy, Tempe, USA

[*] Liuyang.Ding@asu.edu

Abstract

A PTV-based method for estimating high-resolution turbulence statistics is presented, with a focus on the mean velocity, the mean velocity gradient and the isotropic dissipation rate. The theoretical basis of the method is derived from Taylor expansions of velocities and the assumptions that particles are homogeneously seeded and their positions are independent of the flow field. We show that averaging the Taylor expansion equation after some manipulations leads to many desired statistics. In particular, the dissipation estimation relies on the fact that the velocity difference between two closely positioned particles infers the local instantaneous flow strain rate. A PTV simulation using synthetic isotropic turbulence has been performed to validate the method and to understand relevant errors. It is found that the two key parameters that affect the achievable spatial resolution and the accuracy are the total number of sampling times and the seeding density. In addition, the errors associated with particle tracking contribute usually negligible rms fluctuations to the mean velocity and the mean velocity gradient, but they always appear as a positive bias to the dissipation. With the understanding of the errors, we also briefly discuss the strategy to reliably extract a desired statistical quantity.This PTV-based method complements the so-called 'bin-average' method that has been employed to estimate the mean velocity and the Reynold stress. It also opens the way to many other hard-to-measure statistics that are important for understanding and modeling turbulence.

1 Introduction

Dissipation rate is a key statistic for understanding turbulent kinetic energy (TKE) budget, energy cascade and turbulence scaling. The TKE dissipation rate is given by $\epsilon_T = \nu\langle u'_{i,j}u'_{i,j}\rangle + \nu\langle u'_{i,j}u'_{j,i}\rangle$, wherein $u'_{i,j}$ is the derivative of a velocity fluctuation u'_i in the x_j direction; ν is the fluid kinematic viscosity. The first term on the right is the homogeneous isotropic dissipation, while the second term exists only when the flow exhibits inhomogeneity. Precedent studies on dissipation have been mostly conducted with direct numerical simulation (DNS) data (Spalart, 1988; Donzis et al., 2008) for its superior accuracy and accessibility. Reliable measurement of dissipation is yet challenging. A common trouble encountered by virtually any measurement technique that estimates velocity gradients by finite differencing is related to the optimal grid spacing: dissipation is overestimated when the grid spacing is small enough so that the random error in the measurement dominates; if one attempt to reduce the relative random error by increasing the grid spacing, dissipation is underestimated due to unresolved velocity gradient.

In addition to the difficulty in selecting the optimal grid spacing a priori, different measurement techniques also have their own limitations. Traditional point-wise techniques (hot wire anemometry and laser Doppler velocimetry) rely on Taylor's hypothesis to convert temporal derivatives to spatial derivatives. However, the validity of Taylor's hypothesis is not always guaranteed (Dahm and Southerland, 1997), and the resulting accuracy is questionable. Point-wise techniques also face the difficulty of obtaining all nine components of the rate-of-strain tensor, with the exception of multi-sensor probes (Wallace and Vukoslavčević, 2010). PIV allows easy evaluation of spatial derivatives by nature, especially after decades of efforts in advancing PIV towards a fully 3-D, high-spatial/temporal-resolution and high-accuracy tool (Adrian, 2005; Westerweel et al., 2013). However, there are very few successful dissipation

[†]Present address: Department of Mechanical and Aerospace Engineering, Princeton University, Princeton, NJ 08544, USA

measurements by PIV reported in the literature. Many experimentalists have observed underestimated dissipation rate due to the insufficient spatial resolution of correlation-based PIV analysis (Sharp and Adrian, 2001; Tokgoz et al., 2012).

In regard to spatial resolution, particle tracking analysis offers the capability ro resolve a velocity gradient over a length scale of sub-pixel size (Kähler et al., 2012a). Moreover, the developments in camera and laser technologies, in combination with the advances in particle tracking algorithms (Ohmi and Li, 2000; Fuchs et al., 2017) and 3-D particle reconstruction algorithms (Wieneke, 2012; Schanz et al., 2016), enable the performance of PTV to approach or even surpass PIV in many aspects. One promising example is the capability of PTV to obtain high-resolution turbulence statistics, such as the mean velocity (Kasagi and Nishino, 1991; Kähler et al., 2012b) and the Reynolds stress (Discetti et al., 2015). This method has been referred to as the 'bin-average' method or 'ensemble PTV'. The basic idea is to average particle velocities inside individual bins over a large number of ensembles to get the statistical estimate at each bin center. An attractive feature of this method is that the achievable spatial resolution scales inversely with the total number of sampling times, and thus the spatial resolution can be substantially enhanced provided a sufficiently large dataset. It also circumvents the irregularity of PTV data that is not desirable for estimating velocity gradient, vorticity, etc.

In this work, we derive the theoretical basis for the 'bin-average' method that has been employed in a somewhat empirical way in the past. Following the same line, we also extend the method to the estimation of isotropic dissipation rate and mean velocity gradient.

2 Theoretical background

2.1 Mean velocity

Although the validity of estimating the mean velocity by averaging particle velocities inside a subvolume (bin) seems straightforward, the derivation and discussion for the mean velocity provide a more complete picture in terms of the truncation error, the rms error and the optimal subvolume size.

The problem is to estimate the mean velocity at a prescribed location $\boldsymbol{x}^*$ using velocity estimates from tracer particles that randomly occur in a small domain around $\boldsymbol{x}^*$. Suppose, at a sampling time $t^{(q)}$, particle velocity estimates within a cubic domain $\mathscr{D}$ centered at $\boldsymbol{x}^*$ are located at $\boldsymbol{x}^{(p,q)}$, $p = 1, ..., P^{(q)}$. The Taylor expansion of the velocity estimate of the p-th particle, $u_i^{(p,q)} = u_i(\boldsymbol{x}^{(p,q)}, t^{(q)})$, with respect to $\boldsymbol{x}^*$ is

$$u_i^{(p,q)} = u_i^* + u_{i,l}^*(x_l^{(p,q)} - x_l^*) + \frac{1}{2}u_{i,mn}^*(x_m^{(p,q)} - x_m^*)(x_n^{(p,q)} - x_n^*) + \mathscr{O}(L^3) \tag{1}$$

wherein Einstein notation is used, and the superscript asterisks indicate the quantities are taken at $\boldsymbol{x}^*$. The time dependences of asterisked variables are omitted for succinctness, and one should infer they belong to time $t^{(q)}$ in Equation (1) and subsequent equations. We now define a spatial average of a variable $\alpha^{(p,q)}$ for all $\boldsymbol{x}^{(p,q)} \in \mathscr{D}$ at $t^{(q)}$:

$$\prec \alpha^{(p,q)} \succ_{\mathscr{D}} \equiv \frac{1}{P^{(q)}} \sum_{p=1}^{P^{(q)}} \alpha^{(p,q)}. \tag{2}$$

We also define the long time average for a variable $\beta^{(q)}$ in its conventional way:

$$\langle \beta^{(q)} \rangle_{T\to\infty} \equiv \lim_{Q\to\infty} \frac{1}{Q} \sum_{q=1}^{Q} \beta^{(q)} \tag{3}$$

Applying the spatial and time averaging to Equation (1), we eventually obtain

$$\langle \prec u_i^{(p,q)} \succ_{\mathscr{D}} \rangle_{T\to\infty} = \langle u_i^* \rangle + \mathscr{O}(L^2) \tag{4}$$

There are two necessary assumptions used in the derivation of Equation (4). The first one is that flow variables are independent of spatial variables, so, for instance,

$$\langle u_{i,l}^* \prec x_l^{(p,q)} - x_l^* \succ_{\mathscr{D}} \rangle = \langle u_{i,l}^* \rangle \langle \prec x_l^{(p,q)} - x_l^* \succ_{\mathscr{D}} \rangle. \tag{5}$$

The second assumption is homogeneous seeding, so the right hand side of Equation (5) vanishes, and only the second-order term is left in Equation (4). Equation (4) represents a method to estimate the mean velocity with second-order accuracy, namely the truncation error is proportional to L^2.

Moreover, we can subtract the mean gradient term to achieve faster convergence. In principle, the first-order term $\langle u_{i,l}^* \prec x_l^{(p,q)} - x_l^* \succ_{\mathscr{D}} \rangle$ is identically zero when homogeneous seeding is assumed. How-

ever, in a realistic situation when the time/ensemble average is calculated using finite number of samples, it becomes a zero-mean term whose rms fluctuation is proportional to $\langle u^*_{i,l}\rangle$. Therefore, an improved procedure to estimate the mean velocity is to subtract the mean velocity gradient term before time/ensemble averaging, i.e.

$$\begin{aligned}\langle \prec u_i^{(p,q)} - \langle u^*_{i,l}\rangle (x_l^{(p,q)} - x_l^*) \succ_{\mathscr{D}} \rangle &= \langle u_i^*\rangle + \langle u'^*_{i,l}\rangle \langle \prec x_l^{(p,q)} - x_l^* \succ_{\mathscr{D}} \rangle + \mathscr{O}(L^2) \\ &= \langle u_i^*\rangle + \mathscr{O}(L^2) \end{aligned} \tag{6}$$

2.2 Mean velocity gradient

Following the same line, it will be seen that the mean velocity gradient is also obtainable. Subtracting the mean velocity $\langle u_i^*\rangle$ from both sides of Equation (1) and multiplying the equation by $(x_{l'}^{(p,q)} - x_{l'}^*)$ give

$$(u_i^{(p,q)} - \langle u_i^*\rangle)(x_{l'}^{(p,q)} - x_{l'}^*) = u_i'^*(x_{l'}^{(p,q)} - x_{l'}^*) + u^*_{i,l}(x_l^{(p,q)} - x_l^*)(x_{l'}^{(p,q)} - x_{l'}^*) + \mathscr{O}(L^3) \tag{7}$$

Under the same assumptions as stated for the mean velocity, averaging Equation (7) in space and time leads to

$$\begin{aligned}\frac{12}{L^2}\langle \prec (u_i^{(p,q)} - \langle u_i^*\rangle)(x_{l'}^{(p,q)} - x_{l'}^*) \succ_{\mathscr{D}} \rangle_{T\to\infty} &= \frac{12}{L^2}\langle u_i'^*\rangle \langle \prec x_{l'}^{(p,q)} - x_{l'}^* \succ_{\mathscr{D}} \rangle + \langle u^*_{i,l}\rangle \delta_{ll'} + \mathscr{O}(L^2) \\ &= \langle u^*_{i,l'}\rangle + \mathscr{O}(L^2) \end{aligned} \tag{8}$$

wherein $\delta_{ll'}$ is the Kronecker delta arising from the identity $\langle \prec (x_l^{(p,q)} - x_l^*)(x_{l'}^{(p,q)} - x_{l'}^*) \succ_{\mathscr{D}} \rangle = \delta_{ll'} L^2/12$. Here x_l and $x_{l'}$ are also assumed to be independent when $l \neq l'$. Equation (8) represents a method to estimate the mean velocity gradient with second-order accuracy. The mean velocity is subtracted in Equation (8) with a consideration of the rms fluctuation similar to that for the mean velocity. It becomes clear now that the evaluation of the mean velocity and the mean velocity gradient, given in Equation (6) and (8), respectively, can be implemented reciprocally and iteratively to improve their both accuracies.

2.3 Dissipation rate

We now derive the theoretical basis for estimating the isotropic dissipation rate,

$$\epsilon = \nu \langle u'_{i,m} u'_{i,m}\rangle \tag{9}$$

To have the local instantaneous strain rate, we consider the differential between two simultaneous velocity estimates at $\boldsymbol{x}^{(p,q)}$ and $\boldsymbol{x}^{(p',q)}$. Write Equation (1) for both velocities and calculate their difference:

$$u_i^{(p,q)} - u_i^{(p',q)} - \langle u^*_{i,l}\rangle (x_l^{(p,q)} - x_l^{(p',q)}) = u'^*_{i,l}(x_l^{(p,q)} - x_l^{(p',q)}) + \mathscr{O}(L^2). \tag{10}$$

The mean velocity gradient is subtracted from the above equation to reveal the fluctuating velocity gradient responsible for dissipation. For succinctness, we use $G_{\nabla u'_i}$ to denote the left side of Equation (10), i.e.

$$G_{\nabla u'_i} = u_i^{(p,q)} - u_i^{(p',q)} - \langle u^*_{i,l}\rangle (x_l^{(p,q)} - x_l^{(p',q)}) \tag{11}$$

Squaring Equation (10) and averaging in space and time yield

$$\langle \prec G_{\nabla u'_i} G_{\nabla u'_i} \succ_{\mathscr{D}} \rangle_{T\to\infty} = \langle u'^*_{i,m} u'^*_{i,n}\rangle \langle \prec (x_m^{(p,q)} - x_m^{(p',q)})(x_n^{(p,q)} - x_n^{(p',q)}) \succ_{\mathscr{D}} \rangle + \mathscr{O}(L^4), \tag{12}$$

wherein the spatial average of a variable $\alpha^{(p,p',q)} = \alpha(\boldsymbol{x}^{(p,q)}, \boldsymbol{x}^{(p',q)}, t^{(q)})$ involving two positions in $\mathscr{D}$ at the same time $t^{(q)}$ is defined as

$$\prec \alpha^{(p,p',q)} \succ_{\mathscr{D}} \equiv \frac{2}{P^{(q)}\left[P^{(q)} - 1\right]} \sum_{\substack{p,p'=1 \\ p<p'}}^{P^{(q)}} \alpha^{(p,p',q)} \tag{13}$$

If, for a more general case, we specify the size of $\mathscr{D}$ to be $L_1 \times L_2 \times L_3$, then we have the identity

$$\langle \prec (x_m^{(p,q)} - x_m^{(p',q)})(x_n^{(p,q)} - x_n^{(p',q)}) \succ_{\mathscr{D}} \rangle = \delta_{mn} L_m^2/6. \tag{14}$$

Thereby, the homogeneous isotropic dissipation is obtained by letting $L_m = L$:

$$\frac{6}{L^2}\langle \prec G_{\nabla u'_i} G_{\nabla u'_i} \succ_{\mathscr{D}} \rangle_{T\to\infty} = \langle u'^*_{i,m} u'^*_{i,m}\rangle + \mathscr{O}(L^2) = \epsilon + \mathscr{O}(L^2) \tag{15}$$

Equation (11) and (15) represent a method to estimate the homogeneous isotropic dissipation.

3 Numerical validation with synthetic turbulence

3.1 Mean velocity and mean velocigy gradient

We validated the method and studied relevant errors using a PTV simulation with synthetic turbulence. The isotropic synthetic turbulence is generated from the random Fourier model proposed by (Kraichnan, 1970). One of the virtues of the random Fourier model is that many turbulence statistics are well defined, such as the rms velocity, u_{rms}, the transverse Taylor microscale, λ_g, and the dissipation rate, $\epsilon = 15\nu u_{rms}^2/\lambda_g^2$. In addition, a mean shear flow in the x-direction is superposed to the turbulence field to introduce mean velocity gradient. We generated a total of Q = 1e05 independent turbulence fields in a cubic domain of size $10\lambda_g$, i.e. $x, y, z \in [-5\lambda_g, 5\lambda_g]$. Particles are randomly distributed with a seeding density C = 0.55 particles per λ_g^3 cube. 4-pulse particle tracks are calculated for each particle by numerically solving

$$\dot{\boldsymbol{x}}_p(t) = \boldsymbol{u}[\boldsymbol{x}_p(t), t] \tag{16}$$

Three types of error are of our interests in the simulation: (1) rms fluctuation associated with finite time averaging; (2) PTV bias error arising from particle trajectory interpolation; (3) PTV random error due to random particle locating noise. To study the effect of PTV random error, particle positions are perturbed by Gaussian noise with the locating rms error, $(\delta x_p)_{rms}$, ranging from $10^{-4}\lambda_g$ to $10^{-2}\lambda_g$. This corresponds to 1.6e-03 to 1.6e-01 voxel with a reconstruction resolution of 64 vox/mm.

Applying the PTV method to the mean velocity, Figure 1 illustrates the relative mean velocity error, $|\delta_{\langle u\rangle}|/u_{rms}$, as a function of the normalized domain size, L/λ_g. The results from the lowest and the highest locating noise are shown. It is clear that, at relatively large L, the error is dominated by the truncation error and decreases as L^2. When L reduces to below certain value, the error deviates from the L^2 line and starts to raise and wiggle, which is a direct result from the dominance of the rms fluctuation, $(\langle u^*\rangle_T)_{rms}$ ($\langle\cdot\rangle_T$ denotes a finite time average). It is understood that, when L is very small, the number of independent velocity fields in which at least one particle is found in $\mathscr{D}$ dramatically decreases, resulting in poor convergence of the mean and the dominance of $(\langle u^*\rangle_T)_{rms}$. If we assume Poisson distribution for particle occurrence in a given volume, then the rms fluctuation is given by

$$(\langle u^*\rangle_T)_{rms} = \begin{cases} (u_i^*)_{rms}/\sqrt{Q}, & \text{for } \Lambda \gg 1 \\ (u_i^*)_{rms}/\sqrt{QCL^3}, & \text{for } \Lambda \ll 1 \end{cases} \tag{17}$$

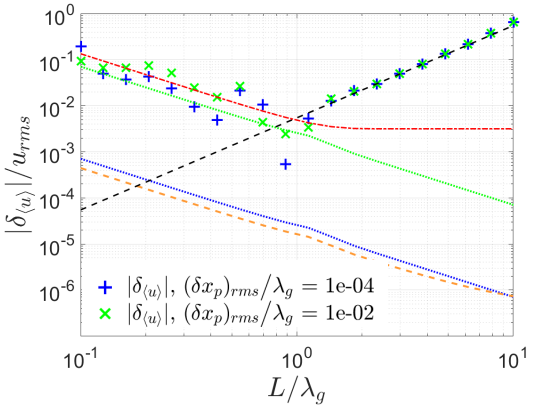

Figure 1: Mean velocity estimation at $(x, y, z) = (0, 0, 0)$. The black dashed line indicates the L^2 trend; the red dash-dot line is $(\langle u_i^*\rangle_T)_{rms}$ given in Equation (17). The green and blue dotted lines are the rms fluctuations of PTV random error at two noise levels; the orange dashed line represents the PTV bias error.

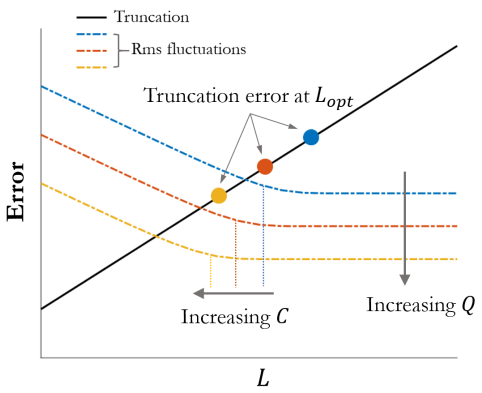

Figure 2: Effects of Q and C on the estimation accuracy. Displayed is in logarithm scale.

wherein $\Lambda = CL^3$ is the averaged number of particles in $\mathscr{D}$. Equation (17) is plotted as the red dash-dot line in Figure 1, which predicts the simulation result well. With the understanding of the competition between the truncation error and the rms fluctuation, the optimal L for evaluating the mean velocity should be taken before the rms fluctuation becomes significant. For the simulation result shown in Figure 1, $L_{opt} \approx 2.5\lambda_g$ and the resulting accuracy is $|\delta_{\langle u \rangle}|/u_{rms} \approx 2\%$. It is also evident in Figure 1 that the PTV random and bias error only contribute rms fluctuations with negligible amplitudes to the mean velocity, even when the locating rms is as high as 0.16 vox ($(\delta x_p)_{rms} = 10^{-4}\lambda_g$). This finding should be generally true in many experiments since nowadays recording highly temporally and spatially resolved PIV data becomes more realistic than ever before.

Based on the above discussion, it now becomes clear that Q and C are two key parameters affecting the achievable accuracy and resolution. Their effects are schematically illustrated in Figure 2: increasing Q lowers the overall rms fluctuation amplitude, and increasing C moves the turning point of $(\langle u_i^* \rangle_T)_{rms}$ ($L_{tp} \sim C^{-1/3}$, see Equation (17)) towards small L. Both of them allow using a smaller L to evaluate the mean velocity, namely improving the accuracy and the spatial resolution. These findings for the mean velocity estimation also apply to the mean velocity gradient.

3.2 Dissipation rate

Figure 3 presents the estimation of dissipation rate from the simulation. At a lower noise level when the PTV error is insignificant (Figure 3a), we observe a similar behavior as in the mean velocity estimation: $\hat{\epsilon}$ ($\hat{[\cdot]}$ denotes an estimated quantity) asymptotically approaches the true value until the rms fluctuation becomes dominant. When the PTV error is considerable, as shown in Figure 3b, it constitutes an always positive bias error that scales as L^{-2}. This is a consequence of the square operation and the multiplication by L^{-2} in the calculation of dissipation (see Equations (12) and (15)). This finding is verified with the simulation result in Figure 3b – if we subtract the L^{-2} PTV error, the same asymptote as in the low noise case is recovered.

The above discussion clearly reveals the importance of reducing PTV error (both bias and random). On the other hand, when experimental conditions do not allow sufficiently low PTV noise, the understanding of the error also suggests a strategy to extract the dissipation rate. In brief, one could use the data at small L to determine the multiplier before L^2, which is an estimate of the PTV error, and subtract the PTV error to obtain the asymptote. The reliability of this strategy relies upon sufficiently large Q and C to mitigate the influence of the rms fluctuation. Our test with the simulation data showed the dissipation error is below 2%, which can be further reduced by increasing Q.

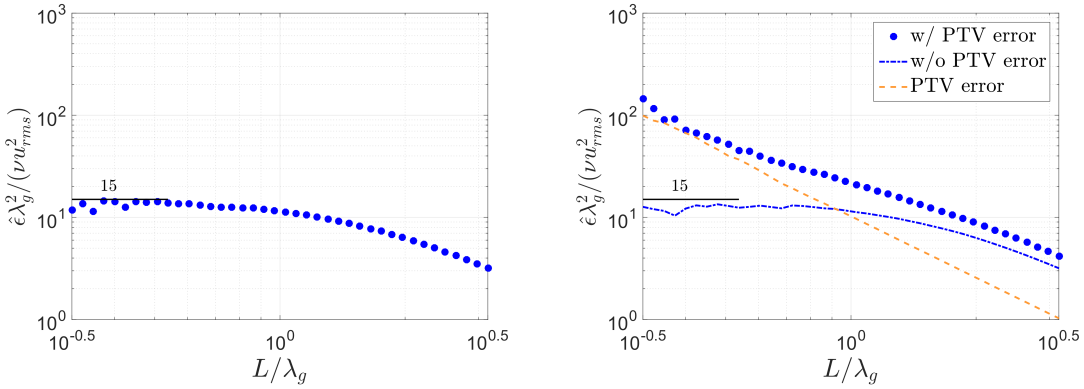

(a) $(\delta x_p)_{rms}/\lambda_g$ = 1.9e-04 (b) $(\delta x_p)_{rms}/\lambda_g$ = 1e-02

Figure 3: Dissipation estimation at different noise levels. The true normalized dissipation, 15, is indicated. The 'PTV error' line in (b) follows L^{-2}.

4 Concluding remarks

As PIV approaches its 35th anniversary, numerous efforts have been made to enable PIV to become a versatile and robust experimental tool for fluid mechanics research. While PIV gained its fame as a velocity field measurement tool, the limitations on spatial resolution compared to point-wise techniques and on data accessibility and accuracy compared to DNS are well recognized. Thanks to the substantial development of PTV techniques, this work demonstrates a good chance for PTV to break through the limitations and become more attractive than ever before.

References

Adrian RJ (2005) Twenty years of particle image velocimetry. *Experiments in fluids* 39:159–169

Dahm WJ and Southerland KB (1997) Experimental assessment of Taylor's hypothesis and its applicability to dissipation estimates in turbulent flows. *Physics of Fluids* 9:2101–2107

Discetti S, Agüera N, Cafiero G, and Astarita T (2015) Ensemble 3D PTV for high resolution turbulent statistics. in *11th international symposium on particle image velocimetry, Santa Barbara, CA USA, September*. pages 14–16

Donzis D, Yeung P, and Sreenivasan K (2008) Dissipation and enstrophy in isotropic turbulence: Resolution effects and scaling in direct numerical simulations. *Physics of Fluids* 20:045108

Fuchs T, Hain R, and Kähler CJ (2017) Non-iterative double-frame 2D/3D particle tracking velocimetry. *Experiments in Fluids* 58:119

Kähler CJ, Scharnowski S, and Cierpka C (2012a) On the resolution limit of digital particle image velocimetry. *Experiments in fluids* 52:1629–1639

Kähler CJ, Scharnowski S, and Cierpka C (2012b) On the uncertainty of digital PIV and PTV near walls. *Experiments in fluids* 52:1641–1656

Kasagi N and Nishino K (1991) Probing turbulence with three-dimensional particle-tracking velocimetry. *Experimental thermal and fluid science* 4:601–612

Kraichnan RH (1970) Diffusion by a random velocity field. *The physics of fluids* 13:22–31

Ohmi K and Li HY (2000) Particle-tracking velocimetry with new algorithms. *Measurement Science and Technology* 11:603

Schanz D, Gesemann S, and Schröder A (2016) Shake-the-box: Lagrangian particle tracking at high particle image densities. *Experiments in fluids* 57:70

Sharp K and Adrian R (2001) PIV study of small-scale flow structure around a rushton turbine. *AIChE Journal* 47:766–778

Spalart PR (1988) Direct simulation of a turbulent boundary layer up to R_θ= 1410. *Journal of fluid mechanics* 187:61–98

Tokgoz S, Elsinga GE, Delfos R, and Westerweel J (2012) Spatial resolution and dissipation rate estimation in taylor–couette flow for tomographic piv. *Experiments in fluids* 53:561–583

Wallace JM and Vukoslavčević PV (2010) Measurement of the velocity gradient tensor in turbulent flows. *Annual review of fluid mechanics* 42:157–181

Westerweel J, Elsinga GE, and Adrian RJ (2013) Particle image velocimetry for complex and turbulent flows. *Annual Review of Fluid Mechanics* 45:409–436

Wieneke B (2012) Iterative reconstruction of volumetric particle distribution. *Measurement Science and Technology* 24:024008